THE JOURNAL OF PHYSICAL CHEMISTRY Letters

pubs.acs.org/JPCL

Comparison of Graphene Growth on Single-Crystalline and Polycrystalline Ni by Chemical Vapor Deposition

Yi Zhang,[†,‡,§] Lewis Gomez,[†,‡,§] Fumiaki N. Ishikawa,[†] Anuj Madaria,[†] Koungmin Ryu,[†] Chuan Wang,[†] Alexander Badmaev,[†] and Chongwu Zhou*[,†,‡]

[†]Department of Electrical Engineering and [‡]Department of Chemistry, University of Southern California, Los Angeles, California 90089, United States

ABSTRACT We report a comparative study and Raman characterization of the formation of graphene on single crystal Ni (111) and polycrystalline Ni substrates using chemical vapor deposition (CVD). Preferential formation of monolayer/bilayer graphene on the single crystal surface is attributed to its atomically smooth surface and the absence of grain boundaries. In contrast, CVD graphene formed on polycrystalline Ni leads to a higher percentage of multilayer graphene (≥3 layers), which is attributed to the presence of grain boundaries in Ni that can serve as nucleation sites for multilayer growth. Micro-Raman surface mapping reveals that the area percentages of monolayer/bilayer graphene are 91.4% for the Ni (111) substrate and 72.8% for the polycrystalline Ni substrate under comparable CVD conditions. The use of single crystal substrates for graphene growth may open ways for uniform high-quality graphene over large areas.

SECTION Nanoparticles and Nanostructures

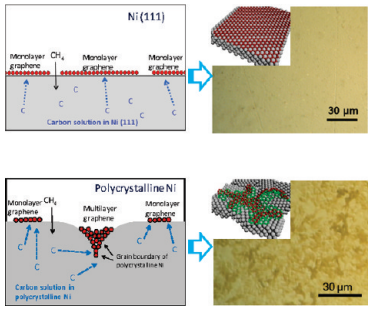

Graphene is a monolayer, two-dimensional material that exhibits exceptionally high crystal and electronic quality.[1] Graphene has attracted great interest because of its outstanding thermodynamic stability, extremely high charge-carrier mobilities, and excellent mechanical stiffness.[2] Tremendous efforts have been made to explore both physical properties[1,3−5] and applications of graphene, such as the opening of bandgap of graphene,[6−9] graphene as transparent conductive electrodes,[10,11] graphene nanomechanical resonators,[12] graphene supercapacitors[13] and so on. Micromechanical cleavage of graphite has allowed the study of fundamental properties of graphene due to the high quality, scarce presence of structural defects, and low levels of unintentional doping of the exfoliated graphene.[14,15] However, this approach is not scalable, and the development of new methods to obtain graphene by scalable methods has surged as an active research area.[16−21]

Recently, chemical vapor deposition (CVD) has raised its popularity in the synthesis of graphene as a scalable and cost-effective approach.[22−29] Polycrystalline Ni has been shown to be a good substrate for graphene synthesis by CVD, but the percentage of monolayer or bilayer graphene is limited by the grain size of crystalline Ni obtained after thermal annealing of Ni thin film.[24,26] It was pointed out that CVD graphene on Ni can be divided into two categories: multilayer graphene (≥3 layers) and monolayer/bilayer graphene, as micro-Raman can distinguish multilayer from monolayer/bilayer, but cannot distinguish monolayer from bilayer.[30] We, among other groups, have reported the synthesis of wafer-scale few-layer graphene by CVD on the surface of polycrystalline Ni.[26] Our results suggest that during the synthesis, carbon atoms tend to segregate on nucleation sites on the Ni surface to form multiple-layer graphene grains. The formation of such multilayer domains is believed to be correlated to different factors including the abundance of defects and grain boundaries on the polycrystalline Ni substrate. It is therefore particularly interesting to investigate the formation of graphene on single crystal Ni due to the absence of interface boundaries, and Ni (111) is especially interesting due to the excellent lattice match between graphene/graphite and Ni (111) face, where the hexagonal lattice constant is 2.497 Å for Ni (111) and 2.46 Å for graphite.[31]

In this work, we report the influence of the concentration of Ni interface boundaries on the formation of such multilayer graphene domains. Synthesis of graphene by CVD on the (111) face of single crystal Ni favors the formation of highly uniform monolayer/bilayer graphene on the Ni surface, and simultaneously hinders the formation of multilayer graphene domains. Our results are understood on the basis of the diffusion-segregation model for carbon precipitation on Ni surface,[32] where the uniform and grain-boundary-free surface of Ni (111) single crystal provides a smooth surface for uniform graphene formation. In contrast, the rough surface of polycrystalline Ni with abundant grain boundaries facilitates the formation of multilayer graphene. Micro-Raman surface mapping reveals that the area percentages of monolayer/bilayer graphene are 91.4% for the Ni (111) substrate

Received Date: August 13, 2010
Accepted Date: October 5, 2010
Published on Web Date: October 11, 2010

DOI: 10.1021/jz1011466 | *J. Phys. Chem. Lett.* **2010**, *1*, 3101–3107

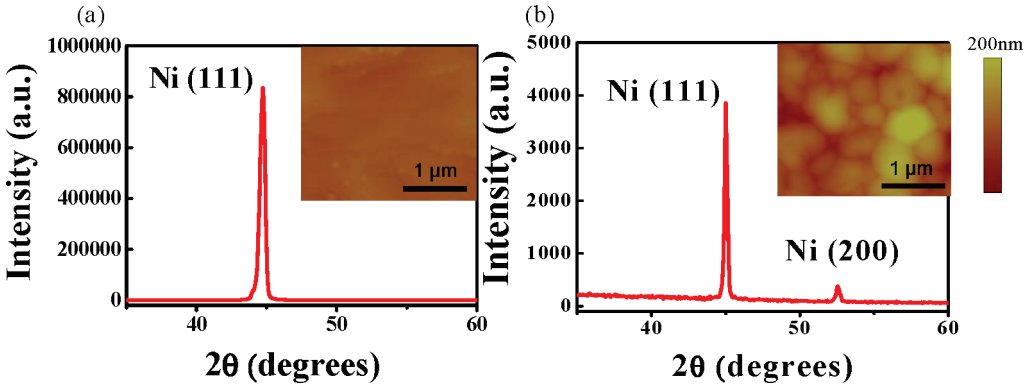

Figure 1. XRD spectra and AFM images (inset) of Ni (111) substrate (a) and polycrystalline Ni substrate (b), respectively. The color scale bar corresponds to the AFM images in insets a and b.

and 72.8% for the polycrystalline Ni substrate under comparable CVD conditions.

To prepare samples for CVD growth, single crystal Ni was obtained from Crystal Base Co., Ltd., while polycrystalline Ni was prepared by depositing 500 nm of Ni metal (99.999% purity) onto a SiO_2/Si wafer by e-beam evaporation. Both the Ni (111) substrate and polycrystalline Ni film substrate were loaded into a CVD chamber. The chamber was heated up to 900 °C under 600 sccm H_2, and the samples were annealed for 15 min under 900 °C. Shown in Figure 1a,b are the X-ray diffraction (XRD) spectra taken after the thermal annealing of both substrates.

There is only a single peak corresponding to Ni (111) in the XRD spectrum taken from the Ni (111) substrate (Figure 1a) as expected. The XRD spectrum of polycrystalline Ni, however, shows a strong Ni (111) peak and a very weak Ni (200) after the annealing process, which indicates the presence of predominantly Ni (111) grains with a smaller population of Ni (100) grains. The atomic force microscopy (AFM) images shown in Figure 1a,b insets further indicate the difference between those two substrates in terms of the surface roughness: The surface of Ni (111) is considerably smoother (average roughness = 5.3 nm) than the polycrystalline Ni (average roughness = 36.3 nm) after thermal annealing. In addition, the polycrystalline Ni surface acquired a multigrain-like appearance after thermal annealing.

The process of graphene growth on Ni can be divided into two parts: the first is carbon segregation from bulk Ni to Ni surface in an intermediate temperature range (~1065−1180 K),[32] and the second is carbon precipitation, which happens when the system temperature decreases (< 1065 K).[32] It is reported that both carbon segregation and precipitation tend to happen at the grain boundaries.[32] The impurities in transition metals tend to segregate at grain boundaries which can be good nucleation sites for carbon segregation.[30] Also, the grain boundaries can act as active sites for the interaction of carbon atoms and lattice vacancies during cooling.[32] Therefore, the grain boundary plays an important role in both the carbon segregation and precipitation.

To fully elucidate the effect of grain boundaries, we have performed a series of experiments to prepare polycrystalline and single crystal Ni samples. Three different annealing rates (175 °C/min, 58 °C/min, 27 °C/min) were chosen from fast to slow for the annealing process of polycrystalline Ni (see Supporting Information), and the medium annealing rate (58 °C/min) was applied to anneal the Ni (111). XRD spectra were collected after the thermal annealing process as shown in Figure 2a. The first three spectra from top to bottom correspond to fast, medium, and slow rate annealing on polycrystalline Ni, and the last one is collected from Ni (111) after annealing. All the spectra were normalized for further analysis. While all four samples show a strong peak corresponding to Ni (111), the polycrystalline Ni samples display an additional Ni (200) peak at $2\theta = 52.16°$, with intensity being highest for fast annealing and lowest for slow annealing. In contrast, the single crystalline Ni XRD spectrum shows no peak for Ni (200) (Figure 2b). Therefore, we can conclude that slower thermal annealing favors the formation of crystalline Ni (111) grains with less grain boundaries for polycrystalline Ni samples.

Graphene was synthesized by CVD at 900 °C at atomosphere pressure, and a cooling rate of 16 °C/min was used down to 500 °C. The details of the synthesis procedures are similar to the previously reported work[26] and can also be found in the Supporting Information. Figure 2c−j depicts the optical images of Ni substrates after graphene synthesis. Figure 2c,d, 2e,f, and 2g,h correspond to polycrystalline Ni samples obtained with fast, medium, and slow thermal annealing rates, respectively. The dark regions are confirmed to consist of multilayer graphene (≥3 layers), while the light regions are confirmed to be monolayer/bilayer graphene using micro-Raman spectroscopy. According to Figure 2c−h, the percentage of multilayer graphene formation increases as the polycrystallinity of the Ni substrate increases. These results suggest that the formation of multilayer graphene can be attributed to the increase of carbon segregation localized at polycrystalline grain boundaries, while the formation of monolayer/bilayer graphene is mainly obtained on the flat central areas of large crystalline grains.

Furthermore, images obtained on Ni (111) substrate after graphene synthesis are shown in Figure 2i,j. Analysis of the graphene growth on single crystal Ni (111) (Figure 2i,j) reveals the scarce formation of multilayer graphene grains. The observation can be understood by considering the absence

DOI: 10.1021/jz1011466 | J. Phys. Chem. Lett. 2010, 1, 3101–3107

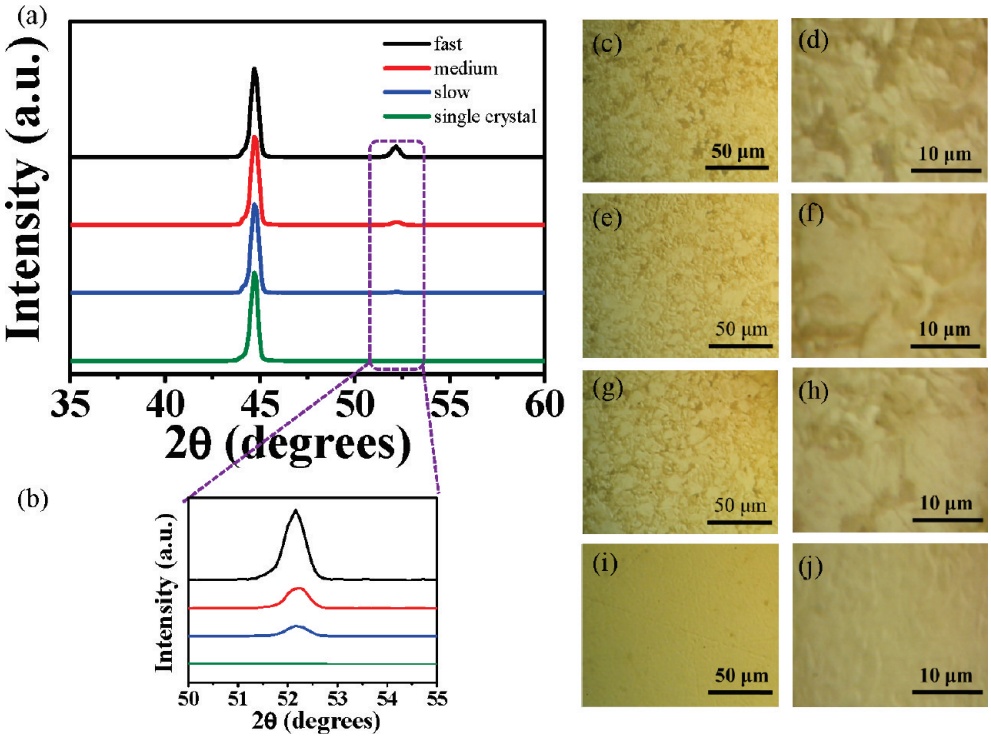

Figure 2. (a) XRD spectra collected from polycrystalline Ni with fast (black), medium (red), and slow (blue) annealing rates and XRD spectrum collected from Ni (111) (green) after thermal annealing (XRD spectrum is identical for Ni (111) using different annealing rates). (b) Zoomed-in XRD spectra of peaks at $2\theta = 52.16°$ (assigned as Ni (200)). (c−j) Optical images taken after graphene CVD growth from polycrystalline Ni with fast (c,d), medium (e,f) and slow (g,h) annealing rates; (i, j) optical images taken after graphene CVD growth from Ni (111).

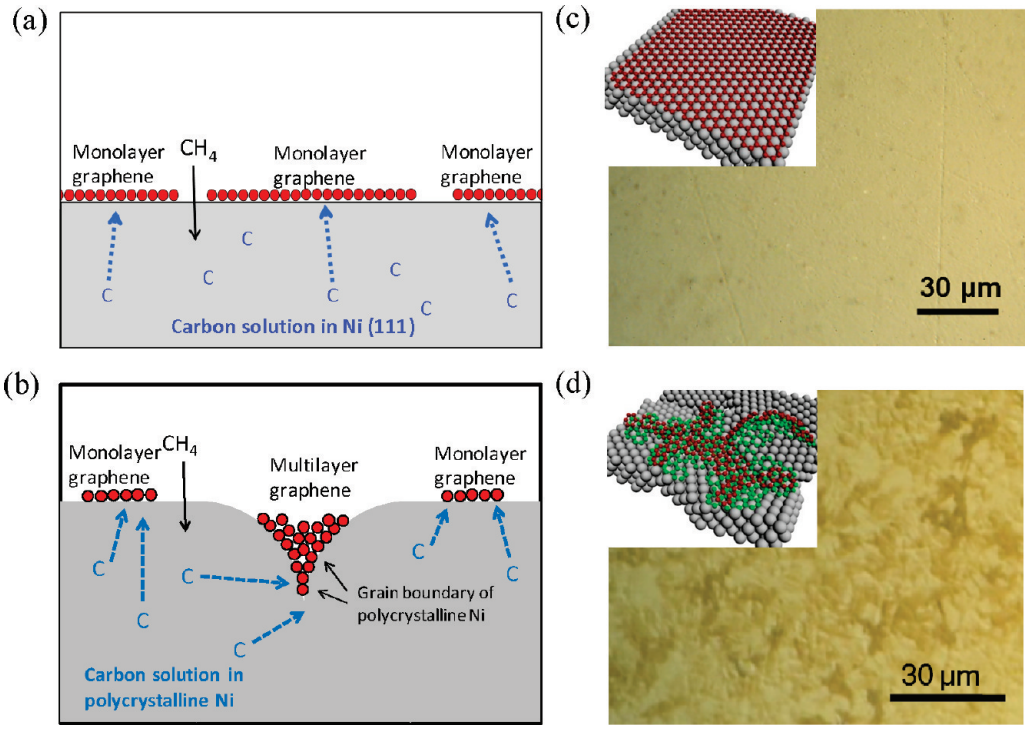

Figure 3. Schematic diagrams of graphene growth mechanism on Ni (111) (a) and polycrystalline Ni surface (b). (c) Optical image of a graphene/Ni (111) surface after the CVD process. The inset is a three-dimensional schematic diagram of a single graphene layer on a Ni (111) surface. (d) Optical image of a graphene/polycrystalline Ni surface after the CVD process. The inset is a three-dimensional schematic diagram of graphene layers on polycrystalline Ni surface. Multiple layers formed from the grain boundaries.

DOI: 10.1021/jz1011466 | J. Phys. Chem. Lett. 2010, 1, 3101–3107

of interplane grain boundaries on the surface of Ni (111) and therefore a shortage of nucleation sites for multilayer graphene formation. Thus, mostly monolayer/bilayer graphene is uniformly formed on the surface of Ni (111) single crystal. Synthesis of graphene utilizing different methane concentrations was also conducted. When a methane concentration of 0.65% was used, the graphene growth was not continuous on either Ni (111) or polycrystalline Ni. Additionally, when we further decreased the methane concentration to 0.50%, no graphene growth was observed on either substrate. On the other hand, when we increased the methane concentration higher than 12% (other growth conditions remained the same), multilayer graphene also formed on Ni (111) substrate.

On the basis of the discussion above, a graphene growth mechanism is proposed in Figure 3.

Figure 3a,b gives schematic diagrams of the possible mechanism of the formation of graphene during the carbon segregation and precipitation on Ni (111) and polycrystalline Ni surfaces, respectively. Due to the high solubility of carbon in Ni, carbon first diffuses into bulk Ni, and then segregates and precipitates onto Ni surface. In the carbon/Ni (111) system, the surface of Ni (111) is very smooth with almost no grain boundaries, allows uniform segregation of carbon onto the Ni (111) surface, and thus tends to form single-layer graphene. In contrast, in the carbon/polycrystalline Ni system, the Ni surface is heavily populated by the grain boundaries, especially interplane grain boundaries, which allow the accumulation of carbon at these sites during the segregation phase and lead to the formation of multilayer graphene.

Optical images were taken from both Ni (111) and polycrystalline Ni substrates. Figure 3c shows that the surface of Ni (111) has a relatively uniform color with only a few dark dots. In contrast, the surface of polycrystalline Ni has many dark grains, as shown in Figure 3d. Both the dark dots and dark grains have been confirmed to be multilayer graphene by micro-Raman, while the rest of the surface is confirmed to be monolayer/bilayer graphene. The scanning electron microscopy (SEM) images also show that the graphene on Ni (111) is much more uniform than graphene on polycrystalline Ni (see Supporting Information). These experimental results match well with our proposed "grain boundary mechanism" for graphene formation. The inset schematic diagram in Figure 3c shows the formation of graphene in an ideal case: a well-ordered graphene sheet on Ni (111) surface without any grain boundaries. The formation of multilayer graphene on polycrystalline Ni is illustrated in the inset of Figure 3d, where red and green represent two graphene layers that segregate and precipitate from grain boundaries. More layers will continue segregating and precipitating from the boundaries depending on the concentration of carbon in bulk Ni. The misalignment between two polycrystalline grains may provide abundant nucleation sites for carbon atoms to segregate from the boundaries. Therefore, multilayer graphene tends to form at the boundaries, while monolayer graphene tends to form on the Ni (111) surface.

The formation of graphene layers on a Ni surface was confirmed by micro-Raman spectroscopy after the CVD process. The information of the defects of graphene, as well as the number of graphene layers can also be derived from Raman spectra. Figure 4a,b shows 10 typical spectra collected from different locations on the synthesized graphene films on Ni (111) and polycrystalline Ni, respectively. The low intensity of the D band (~1350 cm^{-1}) confirms that the graphene formed on both Ni (111) and polycrystalline Ni surfaces is of low defects. Peaks located at ~1590 cm^{-1} and ~2700 cm^{-1} are assigned as G and G′ bands of the graphene layers, respectively. All 10 spectra collected from the graphene on Ni (111) in Figure 4a show single-Lorentzian line shape and narrow line width (25−55 cm^{-1}). Furthermore, all 10 spectra exhibit G′ to G peak intensity ratios ($I_{G'}/I_G$) larger than 1, which are considered fingerprints for the formation of monolayer/bilayer graphene, as previously reported.[24] In contrast, the 10 typical Raman spectra collected from the graphene on polycrystalline Ni in Figure 4b can be divided into two groups.

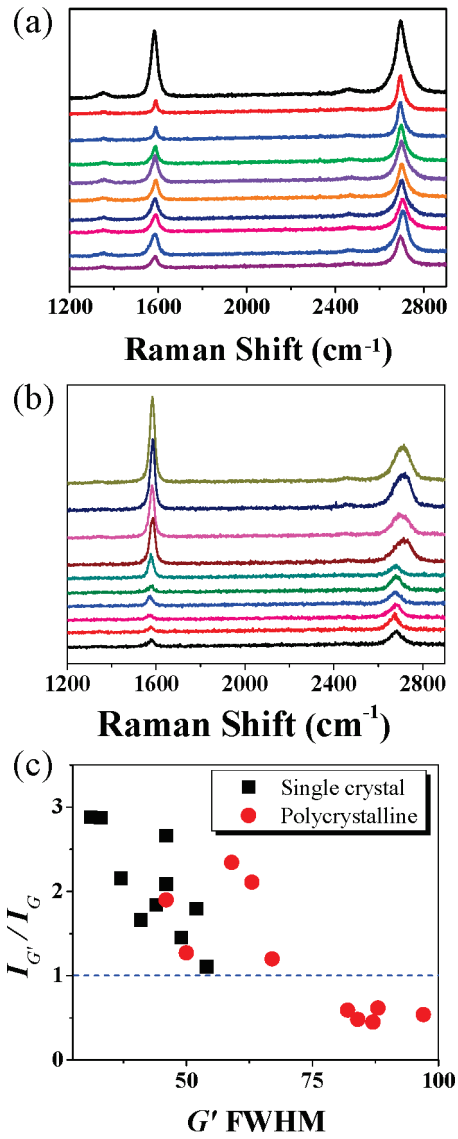

Figure 4. (a,b) Ten typical Raman spectra of graphene grown on Ni (111) and polycrystalline Ni, respectively. (c) The G′-to-G peak intensity ratio ($I_{G'}/I_G$) versus the FWHM of G′ bands of graphene on both Ni (111) and polycrystalline Ni.

DOI: 10.1021/jz1011466 | J. Phys. Chem. Lett. 2010, 1, 3101–3107

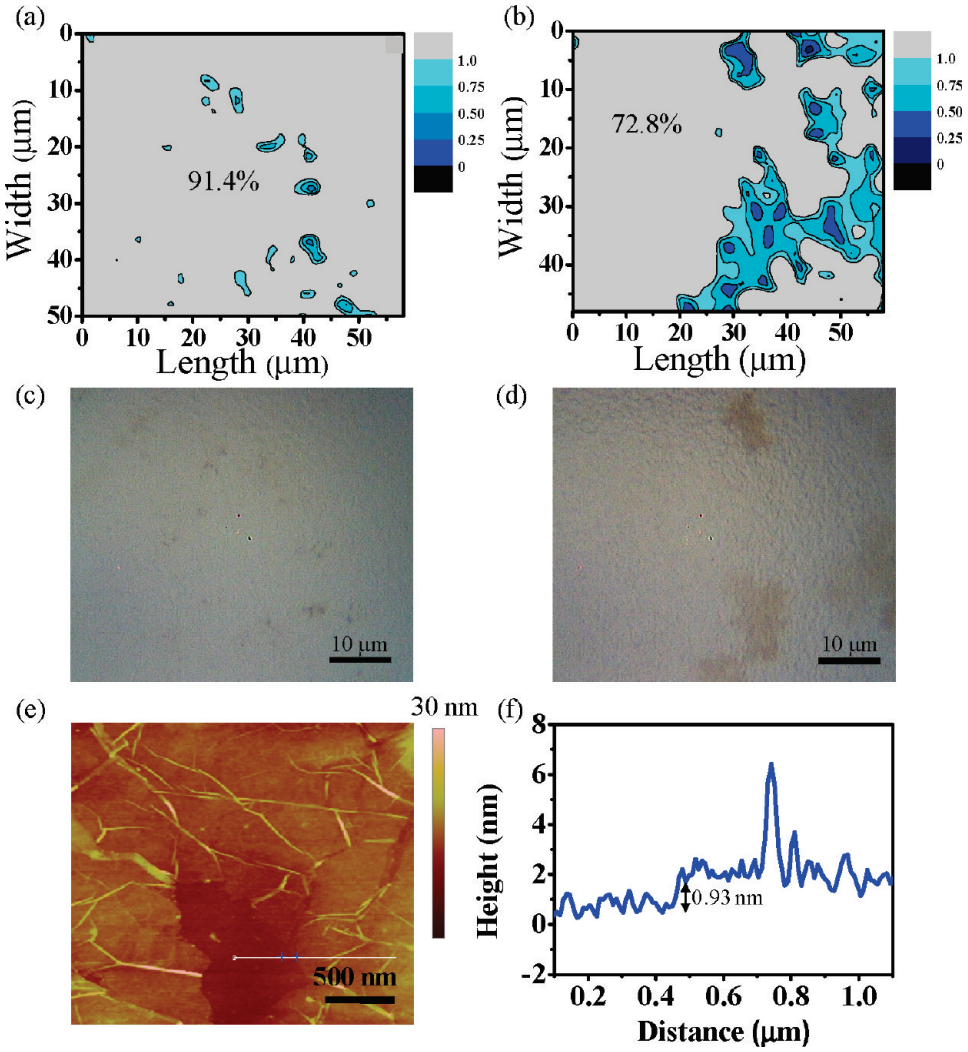

Figure 5. (a) Maps of $I_{G'}/I_G$ of 780 spectra collected on a 60 × 50 μm^2 area on the Ni (111) surface and (b) 750 spectra collected on a 60 × 50 μm^2 area on the polycrystalline Ni surface. Corresponding optical images to Ni (111) Raman map and polycrystalline Ni Raman map (c and d). (e) AFM image of graphene film transferred to SiO_2/Si substrate from Ni (111). (d) Height analysis of the thickness of graphene film.

The first group of spectra are similar to spectra in Figure 4a, which have single-Lorentzian profile for the G′ band, narrow linewiths for G′ peaks, and $I_{G'}/I_G > 1$. On the other hand, the second group of spectra have a noticeable upshift of ~15 cm^{-1} in the G′ band, as well as broadening of G′ band line width (~50 cm^{-1}) that can be fit with four or more Lorentzian peaks.

It is known that the G′ peak position exhibits an upshift with the increase of number of layer of graphene, and the fitting of the G′ peak with two or more Lorentzian peaks is a signature of multilayer graphene.[33,34] Moreover, $I_{G'}/I_G$ for the second group of Raman spectra is smaller than one, which is characteristics of multilayer graphene.[33−35] Altogether, all the Raman spectra collected from the graphene film on single-crystal Ni show the formation of monolayer/bilayer graphene, while only about 50% of the spectra collected from the graphene film grown on polycrystalline Ni correspond to monolayer/bilayer graphene. Figure 4c shows a plot of $I_{G'}/I_G$ values versus full width at half-maximum (FWHM) of G′ bands of micro-Raman spectra taken at random locations on the graphene films grown on single crystal and polycrystalline Ni. It is clearly shown in Figure 4c that all spectra of graphene on single crystal Ni surface have higher $I_{G'}/I_G$ values (all higher than 1) and narrower FWHM, while only half of the spectra of graphene on polycrystalline Ni have high $I_{G'}/I_G$ values and narrow FWHM. Therefore, the result from Figure 3c confirms that the graphene on single crystal Ni is dominantly monolayer/bilayer, while the percentage of multilayer graphene is much higher on polycrystalline Ni.

In order to have a better idea of how the graphene grows in a large area on both Ni (111) and polycrystalline Ni, about 800 Raman spectra were collected over a 3000 μm^2 area with 2 μm spacing between each data point on both surfaces. The $I_{G'}/I_G$ values were then extracted from the spectra. Figure 5a,b shows the $I_{G'}/I_G$ contour maps of graphene on Ni (111) and polycrystalline Ni, respectively. 91.4% of Raman spectra collected from the graphene on Ni (111) surface has $I_{G'}/I_G$ higher than 1, which is a hallmark of monolayer/bilayer graphene.

DOI: 10.1021/jz1011466 | J. Phys. Chem. Lett. 2010, 1, 3101–3107

In contrast, the percentage of monolayer/bilayer graphene is only 72.8% from the graphene grown on polycrystalline Ni. Moreover, the narrow spacing of 2 μm between data points for the Raman measurements enables the confirmation of continuous graphene deposition on both substrates. Figure 5c,d shows the corresponding optical images of the two Raman maps, which are in accordance with the Raman maps: dark regions in the optical images correspond to multilayer graphene in Raman maps, while the rest is confirmed to be monolayer/bilayer graphene.

Furthermore, we transferred graphene to a SiO_2/Si substrate using the same method published in our previous work,[10] and measured the thickness of our graphene film by AFM. Figure 5e shows an AFM image of transferred graphene from Ni (111) substrate. The thickness was measured from the edge of graphene film to the opening (shown in the white line). Figure 5f is the height analysis of the graphene film from the white line drawn on 5e. The thickness of the graphene film is 0.93 nm, which is considered to be one or two layers due to the surface roughness of SiO_2/Si substrate. Graphene from Ni (111) was also transferred to glass for the transmittance measurement to investigate the number of layers of graphene (see Supporting Information). Optical images and Raman spectra were obtained on the transferred graphene film from Ni (111) and polycrystalline Ni film, respectively, for comparison study (see Supporting Information).

In summary, we found that preferential formation of monolayer/bilayer graphene on the single crystal surface is attributed to its atomically smooth surface and the absence of grain boundaries. In contrast, CVD graphene formed on polycrystalline Ni leads to higher percentage of multilayer graphene ($\geq$3 layers), which is attributed to the presence of grain boundaries in Ni that can serve as nucleation sites for multilayer growth. Micro-Raman surface mapping reveals that the area percentages of monolayer/bilayer graphene are 91.4% for the Ni (111) substrate and 72.8% for the polycrystalline Ni substrate under comparable CVD conditions.

SUPPORTING INFORMATION AVAILABLE 1. Graphene growth process. 2. Annealing conditions. 3. SEM and optical images of graphene and micro-Raman spectroscopy on transferred graphene film. 4. TEM image and Electron Diffraction pattern of graphene transferred from Ni (111). 5. Transmittance measurement of graphene transferred from Ni (111). This material is available free of charge via the Internet http://pubs.acs.org

AUTHOR INFORMATION

Corresponding Author:

*To whom correspondence should be addressed. E-mail: chongwuz@usc.edu.

Author Contributions:

§ These authors contributed equally to this work.

ACKNOWLEDGMENT We acknowledge funding from the Focus Center Research Program (FCRP) - Center on Functional Engineered Nano Architectonics (FENA), and the Joint King Abdulaziz City for Science & Technology/California Center of Excellence on Nano Science and Engineering for Green and Clean Technologies. We thank Professor Stephen Cronin for access to the micro-Raman system.

REFERENCES

(1) Geim, A. K.; Novoselov, K. S. The Rise of Graphene. *Nat. Mater.* **2007,** *6*, 183–191.
(2) Obraztsov, A. N. Chemical Vapour Deposition: Making Graphene on a Large Scale. *Nat. Nanotechnol.* **2009,** *4*, 212–213.
(3) Novoselov, K. S.; Geim, A. K.; Morozov, S. V.; Jiang, D.; Zhang, Y.; Dubonos, S. V.; Grigorieva, I. V.; Firsov, A. A. Electric Field Effect in Atomically Thin Carbon Films. *Science* **2004,** *306*, 666–669.
(4) Bolotin, K. I.; Ghahari, F.; Shulman, M. D.; Stormer, H. L.; Kim, P. Observation of the Fractional Quantum Hall Effect in Graphene. *Nature* **2009,** *462*, 196–199.
(5) Novoselov, K. S.; Geim, A. K.; Morozov, S. V.; Jiang, D.; Katsnelson, M. I.; Grigorieva, I. V.; Dubonos, S. V.; Firsov, A. A. Two-Dimensional Gas of Massless Dirac Fermions in Graphene. *Nature* **2005,** *438*, 197–200.
(6) Wang, X. R.; Dai, H. J. Etching and Narrowing of Graphene from the Edges. *Nat. Chem.* **2010,** *2*, 661–665.
(7) Bai, J. W.; Zhong, X.; Jiang, S.; Huang, Y.; Duan, X. F. Graphene Nanomesh. *Nat. Nanotechnol.* **2010,** *5*, 190–194.
(8) Kim, M.; Safron, N. S.; Han, E.; Arnold, M. S.; Gopalan, P. Fabrication and Characterization of Large-Area, Semiconducting Nanoperforated Graphene Materials. *Nano Lett.* **2010,** *10*, 1125–1131.
(9) Wu., M.; Tse, J. S.; Jiang, J. S. Unzipping of Graphene by Fluorination. *J. Phys. Chem. Lett.* **2010,** *1*, 1934–1937.
(10) Gomez, L.; Zhang, Y.; Schlenker, C.; Ryu, K.; Thompson, M.; Zhou, C. W. Continuous, Highly Flexible, and Transparent Graphene Films by Chemical Vapor Deposition for Organic Photovoltaics. *ACS Nano* **2010,** *4*, 2865–2873.
(11) Bae, S.; Kim, H.; Lee, Y.; Xu, X. F.; Park, J. S.; Zheng, Y.; Balakrishnan, J.; Lei, T.; Kim, H. R.; Song, Y. I.; et al. Roll-to-Roll Production of 30-in. Graphene Films for Transparent Electrodes. *Nat. Nanotechnol.* **2010,** *5*, 574–578.
(12) Chen, C. Y.; Rosenblatt, S.; Bolotin, K. I.; Kalb, W.; Kim, P.; Kymissis, I.; Stormer, H. L.; Heinz, T. F.; Hone, J. Performance of Monolayer Graphene Nanomechanical Resonators with Electrical Readout. *Nat. Nanotechnol* **2009,** *4*, 861–867.
(13) Yu, D. S.; Dai, L. M. Self-Assembled Graphene/Carbon Nanotube Hybrid Films for Supercapacitors. *J. Phys. Chem. Lett.* **2010,** *1*, 467–470.
(14) Novoselov, K. S.; Jiang, D.; Schedin, F.; Booth, T. J.; Khotkevich, V. V.; Morozov, S. V.; Geim, A. K. Two-Dimensional Atomic Crystals. *Proc. Natl. Acad. Sci. U.S.A.* **2005,** *102*, 10451–10453.
(15) Meyer, J. C.; Geim, A. K.; Katsnelson, M. I.; Novoselov, K. S.; Booth, T. J.; Roth, S. The Structure of Suspended Graphene Sheets. *Nature* **2007,** *446*, 60–63.
(16) Stankovich, S.; Dikin, D. A.; Piner, R. D.; Kohlhaas, K. A.; Kleinhammes, A.; Jia, Y.; Wu, Y.; Nguyen, S. T.; Ruoff, R. S. Synthesis of Graphene-Based Nanosheets via Chemical Reduction of Exfoliated Graphite Oxide. *Carbon* **2007,** *45*, 1558–1565.
(17) Forbeaux, I.; Themlin, J. M.; Debever, J. M. Heteroepitaxial Graphite on 6H-SiC(0001): Interface Formation Through Conduction-Band Electronic Structure. *Phys. Rev. B* **1998,** *58*, 16396–16406.
(18) Rollings, E.; Gweon, G. H.; Zhou, S. Y.; Mun, B. S.; McChesney, J. L.; Hussain, B. S.; Fedorov, A.; First, P. N.; de Heer, W. A.; Lanzara, A. Synthesis and Characterization of Atomically

Thin Graphite Films on a Silicon Carbide Substrate. *J. Phys. Chem. Solids* **2006,** *67*, 2172–2177.
(19) Hass, J.; Feng, R.; Li, T.; Li, X.; Zong, Z.; de Heer, W. A.; First, P. N.; Conrad, E. H.; Jeffrey, C. A.; Berger, C. Highly Ordered Graphene for Two Dimensional Electronics. *Appl. Phys. Lett.* **2006,** *89*, 143106.
(20) Sutter, P. W.; Flege, J. I.; Sutter, E. A. Epitaxial Graphene on Ruthenium. *Nat. Mater.* **2008,** *7*, 406–411.
(21) Green, A. A. H.; M., C. Emerging Methods for Producing Monodisperse Graphene Dispersions. *J. Phys. Chem. Lett.* **2010,** *1*, 544–549.
(22) Karu, A. E.; Beer, M. Pyrolytic Formation of Highly Crystalline Graphite Films. *J. Appl. Phys.* **1966,** *37*, 2179.
(23) Yu, Q. K.; Lian, J.; Siriponglert, S.; Li, H.; Chen, Y. P.; Pei, S. S. Graphene Segregated on Ni Surfaces and Transferred to Insulators. *Appl. Phys. Lett.* **2008,** *93*, 113103.
(24) Reina, A.; Jia, X. T.; Ho, J.; Nezich, D.; Son, H. B.; Bulovic, V.; Dresselhaus, M. S.; Kong, J. Large Area, Few-Layer Graphene Films on Arbitrary Substrates by Chemical Vapor Deposition. *Nano Lett.* **2009,** *9*, 30–35.
(25) Kim, K. S.; Zhao, Y.; Jang, H.; Lee, S. Y.; Kim, J. M.; Kim, K. S.; Ahn, J. H.; Kim, P.; Choi, J. Y.; Hong, B. H. Large-Scale Pattern Growth of Graphene Films for Stretchable Transparent Electrodes. *Nature* **2009,** *457*, 706–710.
(26) De Arco, L. G.; Zhang, Y.; Kumar, A.; Zhou, C. W. Synthesis, Transfer, and Devices of Single- and Few-Layer Graphene by Chemical Vapor Deposition. *IEEE T. Nanotechnol.* **2009,** *8*, 135–138.
(27) Li, X. S.; Cai, W. W.; An, J. H.; Kim, S.; Nah, J.; Yang, D. X.; Piner, R.; Velamakanni, A.; Jung, I.; Tutuc, E.; et al. Large-Area Synthesis of High-Quality and Uniform Graphene Films on Copper Foils. *Science* **2009,** *324*, 1312–1314.
(28) Li, X. S.; C., W. W.; Colombo, L.; Ruoff, R. S. Evolution of Graphene Growth on Ni and Cu by Carbon Isotope Labeling. *Nano Lett.* **2009,** *9*, 4268–4272.
(29) Levendorf, M. P.; Ruiz-Vargas, C. S.; Garg, S.; Park, J. Transfer-Free Batch Fabrication of Single Layer Graphene. *Nano Lett.* **2009,** *9*, 4479–4483.
(30) Reina, A. T., S.; Jia, X.; Bhaviripudi, S.; Dresselhaus, M. S.; Schaefer, J. A.; Kong, J. Growth of Large-Area Single- and Bi-layer Graphene by Controlled Carbon Precipitation on Polycrystalline Ni Surfaces. *Nano Res.* **2009,** *2*, 509–516.
(31) Eizenberg, M.; Blakely, J. M. Carbon Monolayer Phase Condensation on Ni(111). *Surf. Sci.* **1979,** *82*, 228–236.
(32) Shelton, J. C.; Patil, H. R.; Blakely, J. M. Equilibrium Segregation of Carbon to a Nickel (111) Surface—Surface Phase-Transition. *Surf. Sci.* **1974,** *43*, 493–520.
(33) Ferrari, A. C.; Meyer, J. C.; Scardaci, V.; Casiraghi, C.; Lazzeri, M.; Mauri, F.; Piscanec, S.; Jiang, D.; Novoselov, K. S.; Roth, S.; Geim, A. K. Raman Spectrum of Graphene and Graphene Layers. *Phys. Rev. Lett.* **2006,** *97*, 187401.
(34) Gupta, A.; Chen, G.; Joshi, P.; Tadigadapa, S.; Eklund, P. C. Raman Scattering from High-Frequency Phonons in Supported N-Graphene Layer Films. *Nano Lett.* **2006,** *6*, 2667–2673.
(35) Cancado, L. G.; Reina, A.; Kong, J.; Dresselhaus, M. S. Geometrical Approach for the Study of G′ Band in the Raman Spectrum of Monolayer Graphene, Bilayer Graphene, and Bulk Graphite. *Phys. Rev. B* **2008,** *77*, 245408.

DOI: 10.1021/jz1011466 | *J. Phys. Chem. Lett.* **2010,** *1*, 3101–3107